Modeling Deoxyribose Radicals by Neutralization-Reionization Mass Spectrometry. Part 2. Preparation, Dissociations, and Energetics of 3-Hydroxyoxolan-3-yl Radical and Cation

Shetty Vivekananda,* Martin Sadílek, Xiaohong Chen, Luke E. Adams, and František Tureček

Department of Chemistry, University of Washington, Seattle, Washington, USA

The title radical (**1**) is generated in the gas-phase by collisional neutralization of carbonyl-protonated oxolan-3-one. A 1.5% fraction of **1** does not dissociate and is detected following reionization as survivor ions. The major dissociation of **1** (~56%) occurs as loss of the hydroxyl H atom forming oxolan-3-one (**2**). The competing ring cleavages by O–C-2 and C-4–C-5 bond dissociations combined account for ~42% of dissociation and result in the formation of formaldehyde and 2-hydroxyallyl radical. Additional ring-cleavage dissociations of **1** resulting in the formation of C_2H_3O and C_2H_4O cannot be explained as occurring competitively on the doublet ground (***X***) electronic state of **1**, but are energetically accessible from the ***A*** and higher electronic states accessed by vertical electron transfer. Exothermic protonation of **2** also produces 3-oxo-(*1H*)-oxolanium cation ($\mathbf{3}^+$) which upon collisional neutralization gives hypervalent 3-oxo-(*1H*)-oxolanium radical (**3**). The latter dissociates spontaneously by ring opening and expulsion of hydroxy radical. Experiment and calculations suggest that carbohydrate radicals incorporating the 3-hydroxyoxolan-3-yl motif will prefer ring-cleavage dissociations at low internal energies or upon photoexcitation by absorbing light at ~590 and ~400 nm. (J Am Soc Mass Spectrom 2004, 15, 1068–1079) © 2004 American Society for Mass Spectrometry

Over the years the study of nucleobase and 2-deoxyribose radical intermediates has gained importance owing to their vital role in chemical modifications that occur in the complex process of DNA damage [1]. It is well known that the heterocyclic bases of nucleic acids are important sites of free radical attacks that lead to DNA damage [2]. However, since nucleobases are stacked on the inside of the DNA double strand, a higher proportion of reactive radicals, primarily the hydroxyl radical [3], can be expected to attack the more exposed 2-deoxyribose moieties. It is estimated that about 40% radical attacks cause strand breaks that are presumed to result from reactions involving sugar intermediates formed by hydrogen abstraction from C-1 through C-5 positions in 2-deoxyribose [4]. The radical attacks at the various sites in 2-deoxyribose are thought to occur at random [5, 6] and they result in a variety of stable degradation products [7]. However, little is known about the structure, energetics, and reactivity of reactive intermediates occurring in the early stages of radiation damage.

Investigations in solution found that the anomeric hydrogen at C-1 of 2-deoxyribose is abstracted by a variety of nucleic acid damaging agents [8–12]. In contrast, strand breaks involving ring fission or cleavage of the 3,5′-phosphate ester linkage can be initiated by hydrogen atom abstraction from C-3 in 2-deoxyribose (Scheme **1**). Radicals derived from model oxygen heterocycles have also been studied in solution and the relative rates of H atom abstractions have been measured [13–15].

In contrast to studies in solution which are affected by environmental factors (solvent, radical quenchers, etc.), the rarefied gas phase offers an inherently inert medium in which highly reactive species can be studied in an isolated state. We have previously reported experimental studies that used neutralization-reionization (NR) mass spectrometry [16] to generate heterocyclic

Published online June 9, 2004

Address reprint requests to Dr. F. Tureček, Department of Chemistry, University of Washington, Bagley Hall, Box 351700, Seattle, WA 98195-1700, USA. E-mail: turecek@chem.washington.edu

*Current address: Department of Pharmacology, School of Medicine, New York University, NY 10016.

1044-0305/04/$30.00
doi:10.1016/j.jasms.2004.04.004

Received December 23, 2003
Revised March 29, 2004
Accepted March 29, 2004

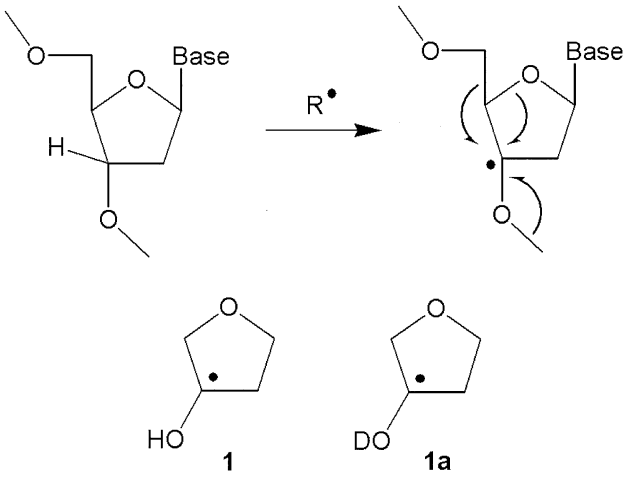

Scheme 1

[17–19], nucleobase [20–22], and phosphate [23] radicals and elucidate their unimolecular dissociations, as reviewed [24]. In the preceding paper in this issue [25], we report on the generation of 2-hydroxyoxolan-2-yl radical which is a simplified model for deoxyribose radicals following hydrogen abstraction at C-1. The present paper uses NR mass spectrometry to generate and investigate the isomeric 3-hydroxyoxolan-3-yl radical (**1**) that mimics deoxyribose radicals formed by hydrogen abstraction at the 3-position, which is critical for strand breaks.

Our experimental approach consists of specific preparation of a stable gas-phase cation ($\mathbf{1}^+$) that has the same bond connectivity as the target radical **1**. Cation $\mathbf{1}^+$ is selected by mass and accelerated to 134,600 ms^{-1} velocity corresponding to an 8150 eV kinetic energy. The cation is discharged by a glancing collision with CH_3SSCH_3 as an electron donor. Because of the short duration of the collision, which is estimated at 7.5 fs from the collision kinematics, the electron transfer is considered to be a vertical process, so that the nascent radical is formed with the geometry of the precursor cation [26]. Unimolecular dissociations of transient radicals are observed on the time scale of 4.4 μs, and the products are analyzed by mass spectrometry following non-selective ionization by collisions with O_2. In addition to product analysis from NR mass spectra, the electronic properties and relative energies of **1** as well as dissociation and transition state energies are obtained by ab initio and density functional theory calculations that are carried out at high levels of theory.

Experimental

Materials

Chemicals (oxolan-3-o1) and reagents were purchased from Sigma-Aldrich (Milwaukee, WI) and used as received. Pure gases (CH_4, CD_4) were purchased from Matheson (Montgomeryville, PA). Oxolan-3-one (**2**) was prepared by oxidation of oxolan-3-ol with pyridinium chlorochromate in dichloromethane, purified by vacuum distillation at 60 torr [27] and analyzed by GCMS. Yield: 45%; 70-eV mass spectrum (*m/z*, rel. intensity): 87 (4.7), 86 (100), 70 (2.4), 58 (52), 57 (14), 56 (5.0), 44(13), 43 (4.4), 42 (6.0), 31 (8.4), 30 (6.9), 29 (20), 28 (83), 27 (14), 26 (9.0).

Measurements

Neutralization-reionization mass spectra were measured on a tandem quadrupole acceleration-deceleration mass spectrometer equipped with electron impact (EI) and chemical ionization (CI) ion sources [28]. Liquid samples were degassed by several freeze-pump-thaw cycles and introduced into the ion source from a glass liquid introduction system at room temperature and 2–3 $\times$ 10^{-6} torr partial pressure. The ion source conditions were as follows. EI: emission current 500 μA, temperature 150–200 °C. CI: emission current 1 mA, temperature 230–250 °C, CI gas pressure 2–3 $\times$ 10^{-4} torr (as measured on an ionization gauge located at the source diffusion pump intake). The ions were extracted from the ion source, passed through the MS-1 r.f.-only quadrupole filter that was tuned to maximize transmission of the ion of interest, and accelerated to 8250 eV. The ions were focused on the neutralization collision cell maintained at 8170 V (negative for cations, positive for anions), where dimethyl disulfide vapor was admitted to achieve 70% transmission of the ion beam. Residual ions were reflected by an electrostatic lens maintained at $\pm$250 V, and the neutral beam was allowed to drift to the reionization cell. Cations were produced by collisions with oxygen at pressures allowing 70% beam transmittance, decelerated to 75-80 eV, energy filtered, and mass analyzed by scanning the MS-2 quadrupole mass filter that was operated to achieve unit mass resolution. The instrument was tuned daily to match the reference NR mass spectrum of CS_2. Variable-time NR mass spectra were measured as described previously [29, 30]. High resolution mass spectra at a resolving power greater than 10,000, and collisionally activated dissociation (CAD) mass spectra were measured on a JEOL HX-110 mass spectrometer at 10 keV ion kinetic energy. Air was used as the collision gas that was admitted in the first field-free region at pressures allowing 70% transmittance of the ion beam. CAD spectra were obtained by scanning the electrostatic and magnet sector while maintaining a constant B/E ratio. The mass resolution in the B/E scans was typically >500. GCMS spectra were measured on an HP-5971A instrument.

Calculations

Standard ab initio and density functional theory (DFT) calculations were performed using the Gaussian 98 suite of programs [31]. Optimized geometries were obtained by DFT calculations using Becke's hybrid

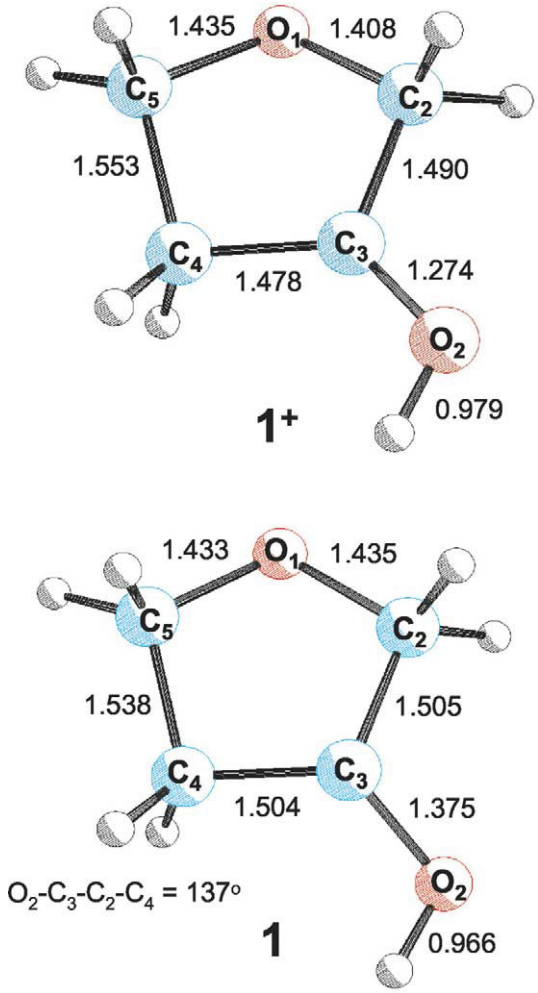

Figure 1. B3LYP/6-31 + G(d,p) optimized Structures of $\mathbf{1}^+$ and **1**. Bond lengths are in angstroms.

functional (B3LYP) [32, 33] and the 6-31 + G(d,p) basis set. The optimized Structures of $\mathbf{1}^+$ and **1** are shown in Figure 1. Complete optimized geometries (Cartesian coordinate format) and harmonic frequencies are available from the corresponding author upon request. Spin unrestricted calculations were performed for all open-shell systems. Spin contamination was small in UB3LYP calculations where the spin operator expectation values $<S^2>$ were 0.75–0.76. Spin contamination in the UMP2 calculations was corrected by applying a spin projection operator (spin annihilation [34, 35]). Stationary points were characterized by harmonic frequency calculations with B3LYP/6-31 + G(d,p) as local minima (all real frequencies) and first-order saddle points (one imaginary frequency). The calculated frequencies were scaled with 0.963 [36] and used to obtain zero-point energy corrections, enthalpies, and RRKM rate constants. Improved energies were obtained by single-point calculations at two levels of theory. Composite G2(MP2) [37] energies were obtained from quadratic configuration interaction calculations with single, double and perturbational triple excitations, QCISD(T) [38] with the

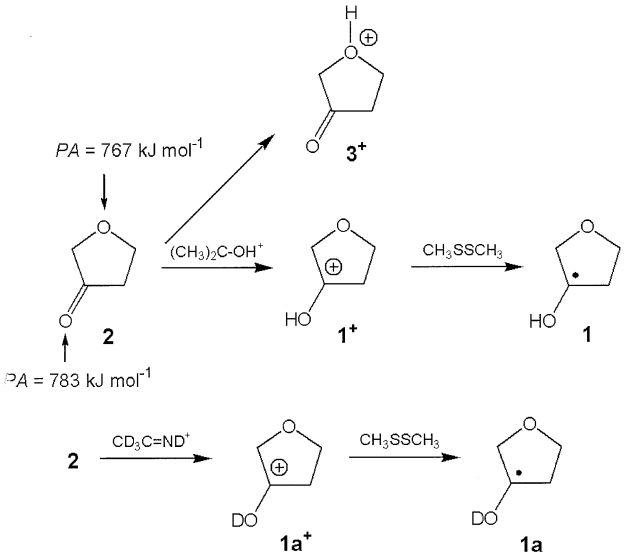

Scheme 2

6-311G(d,p) basis set, and basis set expansions from 6-311G(d,p) through 6-311 + G(3df,2p) via perturbational Moller-Plesset calculations [39], MP2(frozen core). Energies from these high-level calculations are compared to composite B3-MP2 energies that were performed with the 6-311 + G(3df,2p) basis set, as described previously [40–43]. Excited state energies were calculated using time-dependent density functional theory (TD-DFT) [44] with the B3LYP functional [32, 33] and 6-31 + G(d,p), 6-311 + G(2df,p) and 6-311 + G(3df,2p) basis sets. TD-DFT calculations with these basis sets gave excitation energies that were within 0.05 eV for the corresponding electronic states.

RRKM calculations were performed using Hase's program [45] that was recompiled and run under Windows NT [46]. Direct count of quantum states was used in 2 kJ mol^{-1} steps from the transition state energy up to 420 kJ mol^{-1} above it. Rotational states were treated adiabatically. The calculated microscopic rate constants, $k(E,J,K)$, were Boltzmann averaged over the rotational states at 473 K, corresponding to the ion source temperature that defines the precursor ion rotational temperature, to give microcanonical rate constants $k(E)$.

Results and Discussion

Precursor Ion Formation

A possible route to cation $\mathbf{1}^+$ is by gas-phase protonation of oxolan-3-one (**2**, Scheme 2) that can be expected to occur either at the carbonyl or ring ether oxygen depending on their topical proton affinities (PA). The topical PA of the carbonyl oxygen at 298 K was calculated as PA = 783 kJ mol^{-1}, which is greater than that of the ring oxygen which has PA = 767 kJ mol^{-1}. An ion-molecule reaction with $CH_3C{=}NH^+$, generated by CI of acetonitrile (PA(acetonitrile) = 779 kJ mol^{-1})[47], was

Table 1. Collisionally activated dissociation mass spectra of ions $\mathbf{1}^+/\mathbf{3}^+$, $\mathbf{1a}^+/\mathbf{3a}^+$, and $\mathbf{5}^+$. Relative intensity[a]

	$\mathbf{1}^+/\mathbf{3}^+$				$\mathbf{1a}^+/\mathbf{3a}^+$		
m/z	Acetone-CI	CH_3CN-CI	CH_3OH-CI	CH_4-CI	CD_3CN-CI	CD_4-CI	$\mathbf{5}^+$
88	—	—	—	—	—	—	—
87	—	—	—	—	3.3	0.2	—
86	2.5	2.6	2.4	4.0	0.6	0.1	0.6
85	0.5	0.5	0.9	0.7	—	—	2.0
83	—	—	—	—	—	—	3.6
71	0.7	0.2	0.9	0.7	0.4	0.5	3.4
70	0.5	0.1	0.9	0.5	5.0	13.3	—
69	17.3[b]	9.8[b]	7.0[b]	16.5[b]	5.5	15.0	12.6
68	0.5	0.1	1.0	0.5	0.3	—	—
61	—	—	—	—	2.6	0.7	—
60	2.0	1.7	1.4	1.6	7.1	11.8	—
59	8.2	6.3	7.8	8.9	3.3	1.7	7.5
58	3.3	3.7	4.5	3.4	13.2	18.8	1.9
57	20.7	15.1	14.2	18.0	1.5	0.2	6.1
56	0.8	1.3	1.0	1.1	1.0	—	1.6
55	2.0	3.0	2.1	3.1	1.8	—	5.5
54	0.3	—	1.2	—	—	—	1.2
53	0.5	—	1.4	0.9	0.5	—	—
47	—	—	—	—	—	—	—
46	—	—	—	—	3.8	5.6	—
45	3.3	2.6	2.3	3.1	4.3	3.1	15.1
44	1.6	2.2	2.7	1.6	5.0	4.9	0.8
43	5.2	5.4	5.8	5.1	3.8	4.4	9.1
42	1.9	3.1	3.1	2.4	3.0	2.3	2.5
41	6.1	5.4	5.6	4.7	4.5	4.8	4.2
40	1.0	1.6	1.6	1.1	2.5	1.3	1.1
39	3.5	4.8	4.0	3.1	3.8	2.0	2.9
38	1.1	1.8	1.3	1.3	1.5	1.3	0.8
37	0.7	1.5	1.5	1.1	0.4	—	0.6
32	—	—	—	—	5.0	2.7	—
31	4.4	6.2	7.6	3.8	2.8	0.9	2.4
30	1.1	1.8	1.7	1.3	1.8	0.5	0.7
29	4.6	8.2	6.3	4.9	4.3	2.5	4.6
28	1.9	4.0	2.8	2.7	3.0	0.6	2.2
27	2.3	4.4	4.1	2.5	2.5	0.6	4.0
26	1.1	2.3	1.9	1.3	1.8	0.4	2.9

[a]% Relative to sum of CAD fragment intensities.
[b]Major fragments also in metastable-ion spectra.

therefore expected to prefer proton transfer to the carbonyl oxygen forming cation $\mathbf{1}^+$. However, we also observed protonation of **2** by acetone-CI, despite the fact that the difference between the PA of acetone (812 kJ mol^{-1}) [47] and that of the more basic keto group in **2** makes the ion-molecule reaction endothermic. The proton-transfer reaction can possibly be driven thermally at the elevated temperatures (220–250 °C) in the CI ion source and should be selective in producing ion $\mathbf{1}^+$. Gas-phase deuteronation with $(CD_3)_2COD^+$ was used to prepare ion $\mathbf{1a}^+$. Increasingly exothermic protonations with $CH_3OH_2^+$ and CH_5^+ can possibly co-form the less stable, ring-protonated, isomer $\mathbf{3}^+$, as will be discussed later.

Precursor Ion Dissociations

The ions prepared by protonation of **2** were characterized by accurate mass measurements (measured 87.0441, $C_4H_7O_2$ requires 87.0446) and CAD spectra.

The latter were found to depend only weakly on the gas-phase acid used to protonate **2**. The CAD spectra show dissociations by loss of H (*m/z* 86), water (*m/z* 69), C_2H_4 (*m/z* 59), CH_2O (*m/z* 57) and ketene (*m/z* 45) (Table 1). OD-labeling in $\mathbf{1a}^+$ revealed clean eliminations of light C_2H_4 and CH_2O, whereas the loss of water involved H_2O and HDO in a 1.1:1 ratio. These dissociations are compatible with both Structures $\mathbf{1}^+$ and $\mathbf{3}^+$ and do not allow us to distinguish whether a single ion structure or a mixture of tautomers was produced upon protonation of **2**. However, isomer distinction is achieved by $^+NR^+$ mass spectra, as discussed later. The ions which are likely to contain both $\mathbf{1}^+$ and $\mathbf{3}^+$ are denoted as $\mathbf{1}^+/\mathbf{3}^+$ and likewise for the corresponding radicals.

We also made an attempt to prepare ion $\mathbf{1}^+$ by another pathway, which was thought to occur by dissociative ionization of 3-*n*-propyloxolan-3-ol (**4**, path ***a***, Scheme 3). Although a $C_4H_7O_2^+$ ion of the correct elemental composition is formed with a reasonable relative intensity (20%) upon loss of C_3H_7 from **4**, its CAD and $^+NR^+$ mass

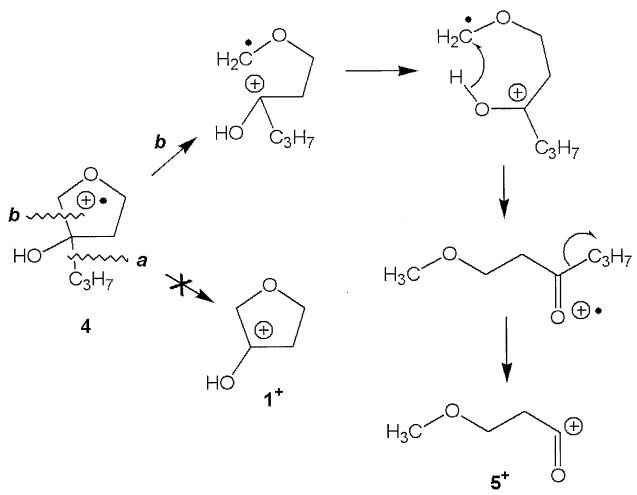

Scheme 3

spectra indicate that a yet different isomer, 3-methoxypropionyl cation $\mathbf{5}^+$, is formed through path ***b***. Evidence for Structure $\mathbf{5}^+$ follows from the CAD spectrum (Table 1) that displays peaks due to losses of H_2, $2H_2$, CH_4 (CH_3D from **4**-OD), water, CO, CH_2O, methanol, and a major peak of $CH_3OCH_2^+$ due to loss of ketene.

Dissociations of Radicals ***1, 1/3,*** *and* ***1a/3a***

The $^+NR^+$ spectrum of $\mathbf{1}^+$ (Figure 2a) shows a well defined survivor ion at *m/z* 87 and fragments at *m/z* 86 (loss of H), 58 (loss of H and CO), 57, 55, 44, 43, 42, and the dominant group of C_2H_x (x = 1–4) and CH_xO (x = 0–3) at *m/z* 26–31. Some of these fragments can be explained by post-reionization dissociations of the survivor ion. However, the major ion fragment in the CAD spectrum of $\mathbf{1}^+$ (*m/z* 69) and its corresponding neutral counterpart (H_2O at mass 18) are not abundant in the $^+NR^+$ spectrum of $\mathbf{1}^+$. This indicates that most of the $^+NR^+$ fragments arise by dissociations originating from **1**. Loss of the hydroxyl hydrogen forms oxolan-3-one (**2**), which is identified by its survivor ion at *m/z* 86 and the *m/z* 58, 57, 56, 44, 42, 29, and 28 fragments in its $^+NR^+$ spectrum that resembles the EI mass spectrum (the reference $^+NR^+$ spectrum of **2** is not shown here). In addition to these, the $^+NR^+$ spectrum of $\mathbf{1}^+$ contains fragments at *m/z* 44 (loss of 43 u) and 43 (loss of 44 u) that are complementary by mass, arise neither by CAD

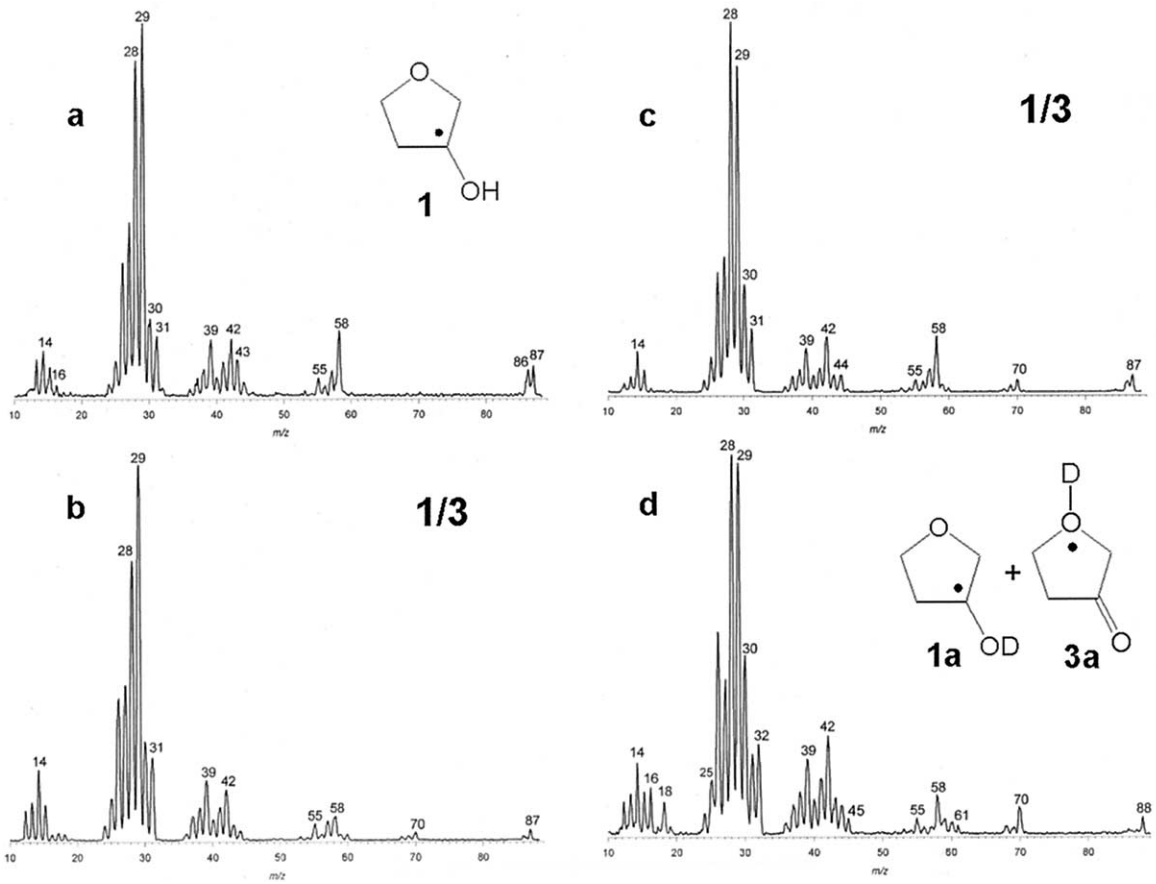

Figure 2. Neutralization (CH_3SSCH_3, 70% transmittance)-reionization (O_2, 70% transmittance) spectra of (**a**) $\mathbf{1}^+$ prepared by protonation with acetone-CI, (**b**) $\mathbf{1}^+/\mathbf{3}^+$ prepared by protonation with CH_3CN-CI, (**c**) $\mathbf{1}^+/\mathbf{3}^+$ prepared by protonation with CH_4-CI, (**d**) $\mathbf{1a}^+/\mathbf{3a}^+$ prepared by deuteronation with CD_3CN-CI.

of $\mathbf{1}^+$ nor by $^+NR^+$ of **2**, and therefore must be due to dissociations of radical **1**.

The $^+NR^+$ spectra of ions prepared by exothermic protonation of **2** with CH_3CN-CI and CH_4-CI (Figure 2b and c) show new dissociation products that were absent in the spectrum of $\mathbf{1}^+$. The new fragments appear at *m/z* 70 (loss of OH), 69, 68, 60 (loss of C_2H_3), and 59 (loss of C_2H_4/CO). The relative abundance of the *m/z* 68-70 peaks increases with the exothermicity of gas-phase protonation from CH_3CN-CI to CH_4-CI. $^+NR^+$ mass spectra of ions prepared by gas-phase deuteronation with CD_3CN-CI (Figure 2d) and CD_4-CI ($\mathbf{1a}^+/\mathbf{3a}^+$) show no mass shifts of the *m/z* 68–70 peaks, which indicates that the D atom is lost cleanly within the OD group. In contrast, the *m/z* 59 and 60 peaks show retention of deuterium as evidenced by the corresponding mass shifts to *m/z* 60 and 61, respectively. Noteworthy is the substantial decrease in intensity of the *m/z* 87 and 86 peaks due to loss of H and D, respectively. This indicates that (1) the hydroxyl hydrogen is lost preferentially, and (2) when replaced by D, its loss is affected by substantial isotope effects in **1a**/**3a**. These $^+NR^+$ mass spectrometric data can be interpreted by co-formation together with $\mathbf{1}^+$ of the isomeric 3-oxo-(*1H*)-oxolanium cation ($\mathbf{3}^+$) upon exothermic protonation of **2**. The 3-oxo-(*1H*)-oxolanium radical **3** formed by neutralization of $\mathbf{3}^+$ is a hypervalent species whose unimolecular dissociations can be expected [48–53] to differ from those of **1**, as indeed observed.

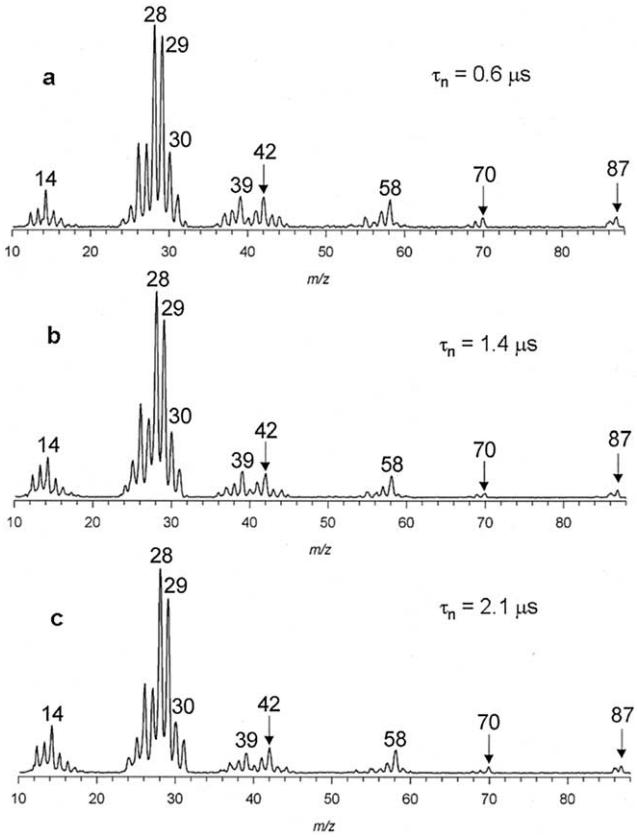

Figure 3. Variable-time NR mass spectra (CH_3SSCH_3, 70% transmittance/O_2, 70% transmittance) of $\mathbf{1}^+/\mathbf{3}^+$. The neutral lifetimes were (**a**) 0.6 μs, (**b**) 1.4 μs, and (**c**) 2.1 μs.

*Variable-Time NR^+ Mass Spectra of **1/3***

Further information about unimolecular dissociations of **1**/**3** was sought from the dissociation kinetics of neutral intermediates, as probed by variable-time $^+NR^+$ mass spectra. In these measurements, the times for dissociations of radicals (t_1) and their reionized counterparts (t_2) are varied simultaneously but in an opposite manner, such that the total time $t = t_1 + t_2$ remains constant. The variable-time $^+NR^+$ mass spectra (Figure 3) showed only minor changes when the dissociation times for neutrals were varied from 0.6 μs (top spectrum) to 2.1 μs (bottom spectrum). Changes are observed in the intensity ratios [**1** − H]/[**1**], and [*m/z* 31]/[*m/z* 30] that both increase at longer dissociation times for neutrals. These indicate that there is a fraction of metastable radicals **1** that dissociate by loss of H on the microsecond time scale. The increased formation of CH_2OH is less straightforward to interpret because the fragment may be formed by consecutive dissociations of neutral intermediates or after reionization. The dissociation mechanisms for **1** and **3** were further investigated by ab initio-RRKM calculations, as discussed next.

*Dissociation Energies and Mechanisms for Radicals **1** and **3***

To interpret the dissociations observed in the $^+NR^+$ spectra we investigated computationally the relevant parts of the potential energy surfaces (PES, Figure 4) to obtain transition state and dissociation energies. Vertical neutralization of $\mathbf{1}^+$ is accompanied by only moderate Franck-Condon effects, as judged from the calculated adiabatic and vertical ionization energies of **1**, IE_a = 6.43 and IE_v = 7.32 eV, respectively, and the vertical recombination energy of $\mathbf{1}^+$, RE_v = 6.01 eV. The vibrational excitation in **1** due to Franck-Condon effects is estimated at 37 kJ mol^{-1}.

Intuitively, one can expect the radical center at C-3 to destabilize the bonds originating at the adjacent atoms, e.g., the O–H, O-1–C-2, and C-4–C-5 bonds in **1**. The PES for dissociations of **1** (Figure 4) shows the lowest energy in **TS1** for cleavage of the O-1–C-2 bond at E_{TS1} = 118 kJ mol^{-1} for the G2(MP2) value. This bond dissociation forms an open-ring-intermediate (**5**) which is 59 kJ mol^{-1} less stable than **1**. Radical **5** can undergo direct cleavage of the C-4–C-5 bond through **TS2** forming formaldehyde and 2-hydroxyallyl radical. Note that the overall dissociation energy for this pathway is only 41 kJ mol^{-1} relative to **1**. An energetically still more favorable pathway is via internal rotation in **5** (**TS3**) to form the hydrogen-bonded conformer **6**, which can dissociate to formaldehyde and 2-hydroxyallyl radical through **TS4** at E_{TS4} = 80 kJ mol^{-1} (Figure 4). Note that the **TS2**–**TS4** energies are below that for **TS1**, indicating that the latter defines the rate-determining step in this dissoci-

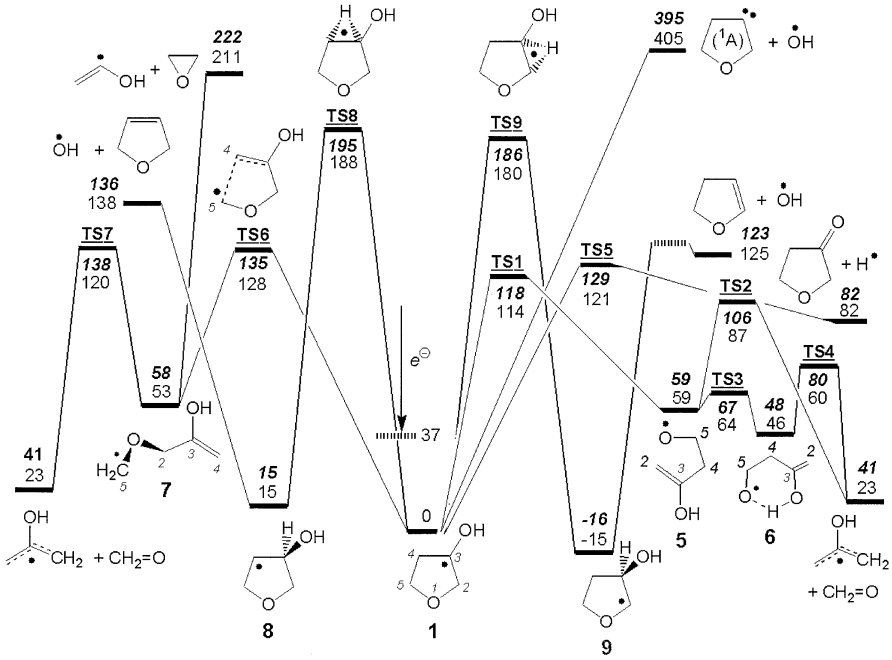

Figure 4. Schematic potential energy surface for dissociations and isomerizations of **1**. The energies in kJ mol^{-1} were corrected for zero-point contributions and refer to 0 K. Roman numerals: B3-PMP2/6-311 + G(3df,2p) relative energies. Bold italics: G2(MP2) relative energies.

ation pathway. A competitive pathway for dissociation of **1** is by cleavage of the O–H bond to form **2**, which requires a slightly higher energy in **TS5** (E_{TS5} = 129 kJ mol^{-1}) than does **TS1**. The 0 K thermochemical threshold for this loss of H is at 82 kJ mol^{-1}. A third pathway commences by cleavage of the C-4–C-5 bond in **1** to form another open-ring intermediate (**7**). The energy barrier for this bond cleavage is E_{TS6} = 135 kJ mol^{-1} in **TS6**. Radical **7** can dissociate by cleavage of the C-2–O-1 bond through **TS7** at E_{TS7} = 138 kJ mol^{-1}, forming the 2-hydroxyallyl radical and formaldehyde. It is noteworthy that although the products of this dissociation pathway through **TS6** → **TS7** and those through **TS1** → **TS2** (or **TS3** and **TS4**) are identical, the order of consecutive bond dissociations is energetically more favorable in the latter path, which should be also kinetically preferred.

The PES in Figure 4 also provides an unequivocal answer to the question of OH loss from **1**. Direct cleavage of the C-3–OH bond in **1** would result in the formation of a high energy singlet oxolane-3-carbene which is 395 kJ mol^{-1} endothermic (the triplet carbene is still 57 kJ mol^{-1} higher in energy) and cannot compete with the other dissociations of **1**. Hence, the direct path for OH loss from **1** is improbable on energy grounds. An activation of the C-3–O bond can occur in isomeric radicals **8** and **9** which are, respectively, 15 kJ mol^{-1} less stable and 16 kJ mol^{-1} more stable than **1**. Loss of OH from **8** and **9** would form, respectively, 3-oxolene with $\Delta H_{rxn,0}$ = 136 kJ mol^{-1} and 2-oxolene with $\Delta H_{rxn,0}$ = 123 kJ mol^{-1}. However, the 1,2-hydrogen migrations in **1** forming **8** and **9** have prohibitively high transition state energies (**TS8** and **TS9**) that were calculated as E_{TS8} = 195 kJ mol^{-1} and E_{TS9} = 186 kJ mol^{-1}. Hence, these rearrangements are not expected to be kinetically competitive with the simple bond dissociations through **TS1**, **TS5**, and **TS6**.

The loss of OH can be best explained by occurring in a transient hypervalent oxonium radical (**3**) produced by vertical neutralization of **3**$^+$. Calculations show that vertically formed **3** is a high-energy species that spontaneously dissociates by O–C-2 bond cleavage forming 4-hydroxy-2-oxyallyl radical (**10**, Figure 5). It may be noted that analogous C–O bond dissociations have been reported for hypervalent oxonium radicals derived from aliphatic ethers [50–52]. Radical **10** is produced with 283 kJ mol^{-1} internal energy and is presumed to dissociate rapidly by OH loss forming cyclobutanone or 2-methyleneoxetane (**12**) as stable products. The thermochemical threshold for the formation of **12** was calculated at 182 kJ mol^{-1} and is thus energetically accessible from **3**. Another energetically feasible pathway is by internal rotation in **10** to form the more stable conformer **11**, which can dissociate through **TS10** (E_{TS10} = 91 kJ mol^{-1}) to form ketene and 2-hydroxyethyl radical at a 82 kJ mol^{-1} threshold energy. Interestingly, the potential energy surfaces for dissociations of **1** and **3** can be interconnected via **TS11** for hydrogen migration between O-1 and O-2 that interconverts radicals **6** and **11** (Figure 5). Noteworthy is the substantially greater stability (by 97 kJ mol^{-1} at 0 K) of the enoloxy radical **11** compared to the alkoxy radical **6** that can be attributed to π-conjugative stabilization in **11**.

*Excited States of **1***

An intriguing feature of the $^+NR^+$ spectrum of **1** is that the survivor ion represents only a small fraction (1.5%)

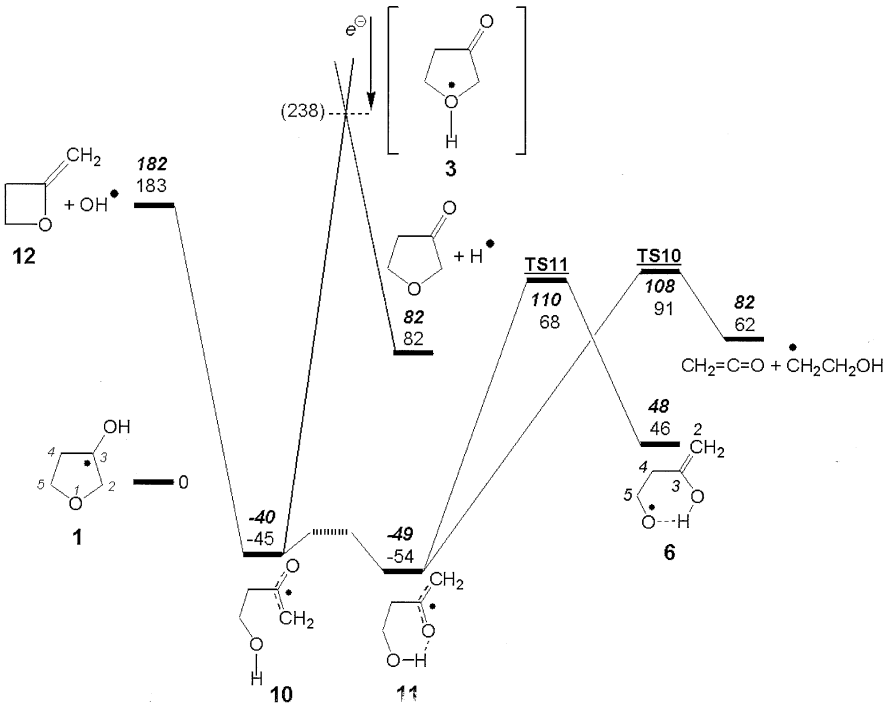

Figure 5. Schematic potential energy surface (in kJ mol^{-1}) for dissociations of **3**. Except for vertically formed **3** which is not an energy minimum, the energies were corrected for zero-point contributions and refer to 0 K. Roman numerals: B3-PMP2/6-311 + G(3df,2p) relative energies. Bold italics: G2(MP2) relative energies.

of the total ion intensities. This, together with the fact that the $^{+}NR^{+}$ spectrum does not show products of the lowest-energy ion dissociation by water elimination, indicates extensive dissociations of radicals **1** formed by vertical electron transfer. The variable-time spectra show that the dissociations of the neutral intermediates mostly occur on the time scale shorter than 0.6 μs, which is consistent with the steep rise with internal energy of the log *k* curves for the competing reactions (vide infra). However, radical **1** is calculated to be a bound species, and the vibrational excitation it receives through Franck-Condon effects (37 kJ mol^{-1}), even when combined with the precursor ion internal energy (36 kJ mol^{-1} at 523 K), should be insufficient to drive dissociations that require substantially higher energies even in the lowest transition states (Figure 4). Moreover, the formation of C_2H_3O and C_2H_4O fragments on NR is incompatible with the potential energy surface in Figure 4, which places the threshold energy for this dissociation at 222 kJ mol^{-1}, way above the other relevant and experimentally observed dissociations. Hence, the PES in Figure 4 does not explain the formation of the C_2H_3O and C_2H_4O fragments in the $^{+}NR^{+}$ spectrum.

In collisions occurring on the femtosecond time scale, electron transfer can occur between the donor's highest occupied molecular orbital (HOMO) and any of the unoccupied molecular orbitals of the electron acceptor [16a, 54]. Thus, electron transfer can result in radical **1** being formed in the ground doublet electronic state (***X***) (Figure 4), or in an *excited doublet state*. We examined by TD-B3LYP calculations the excited states in **1** formed by vertical electron transfer to $\mathbf{1}^{+}$ as shown in Figure 6 for the lowest three excited states. These states all arise by excitation of an electron from the 24α singly-occupied molecular orbital (SOMO), which is a π-orbital that is delocalized in an anti-bonding fashion over C-3, OH, and the C-2 and C-4 methylene groups in **1** (Figure 7). These outer excited states are long lived, as their radiative lifetimes are calculated as 3.5, 0.6, and 2.3 μs, for transitions to the ***X*** state from the ***A***, ***B***, and ***C*** states, respectively. Interestingly, radical **1** is expected to weakly absorb light in the visible region to produce the ***A*** and ***B*** states at λ = 592 and 403 nm, respectively. The excitation energies indicate that, starting with the ***A*** state, vertically formed **1** would have a sufficient internal energy to dissociate to C_2H_3O and C_2H_4O. The formation of these products thus can be attributed to the formation of excited electronic states upon vertical electron transfer.

Figure 6 shows the excited state energies along the reaction coordinates corresponding to 1,2-H atom migrations through **TS8** and **TS9**, which are relevant to the formation of isomeric radicals **8** and **9** as potential intermediates for loss of OH from **1**. However, the excited state energies increase sharply for vertical excitations in **TS8** and **TS9**, such that the energy gaps for ***X*** $\rightarrow$ ***A***, ***B***, ***C*** are greater in **TS8** and **TS9** than they are in **1**. This means that 1,2-H atom migrations in **1** are made even less facile in excited electronic states, and the loss of OH must be attributed to a dissociation of an isomeric species, such as **3**, as discussed above.

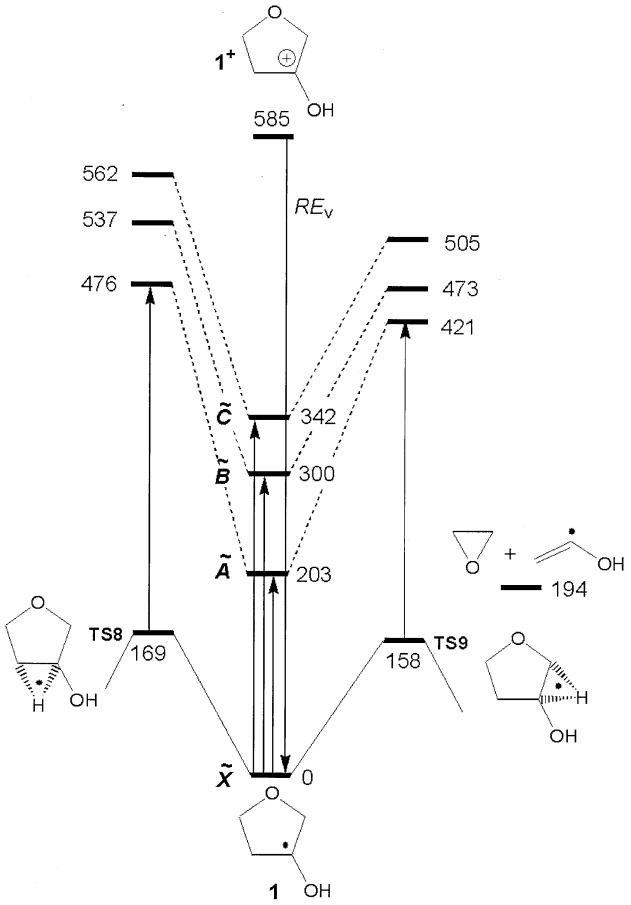

Figure 6. Energy diagram for vertical electron excitations in **1**, **TS8**, and **TS9**. Energies in kJ mol^{-1} from TD-B3LYP/6-311 + G(2df,p) calculations.

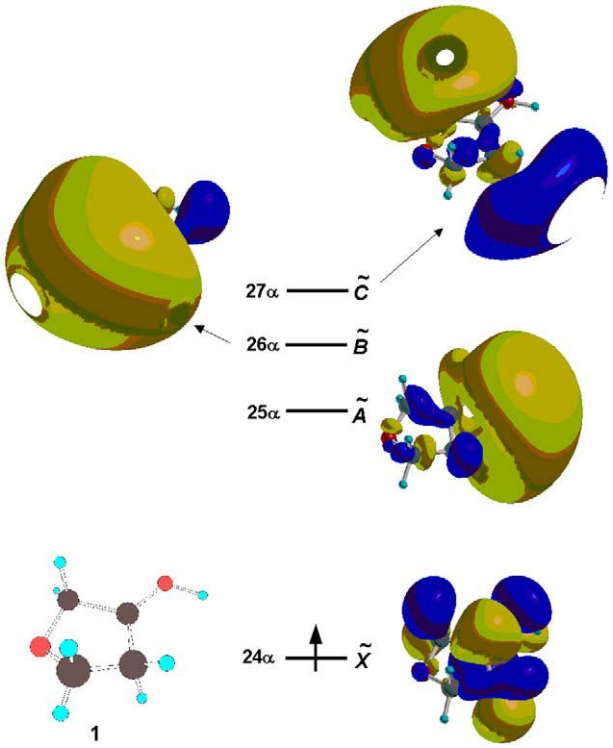

Figure 7. Molecular orbitals in the ***X***, ***A***, ***B***, and ***C*** states of **1**. The corresponding CI coefficients for the excitations as calculated by TD-B3LYP/6-311 + G(2df,p) were as follows: 1.000 (24$\alpha \rightarrow$ 25α) for the ***A*** state, 0.979 (24$\alpha \rightarrow$26α) − 0.107 (24$\alpha \rightarrow$30α) − 0.123 (24$\alpha \rightarrow$ 31α) for the ***B*** state, and 0.988 (24$\alpha \rightarrow$ 27α) for the ***C*** state.

RRKM Kinetics

The TS energies for the ground electronic state of **1** were further used for RRKM calculations of unimolecular rate constants for competitive dissociations. The dissociations involving ring cleavages in **1** are two-step or multiple-step reactions so that the overall kinetics should also include the rate constants for the reverse ring closures, e.g., **5** → **1** and **7** → **1** (Scheme 4). In the first approximation, we neglect the fast isomerization of intermediates **5** ↔ **6** that according to Figure 4 proceeds through **TS3** with negligible energy barrier (8 kJ mol^{-1}), and we treat the kinetics according to Scheme 4. RRKM rate constants were calculated for all steps in Scheme 4 using the G2(MP2) and B3-PMP2 PES; the rate constants for the O–H, O–C-2 and C-4–C-5 bond dissociations in **1** are shown as log k in Figure 8. The dissociation of the O–C-2 bond has the lowest TS energy and dominates at low excitations of **1**. However, the log k curves for k_{O-H} and k_{O-C-2} cross at 190 kJ mol^{-1} (152 kJ mol^{-1} by B3-PMP2), above which energy the loss of H is faster. The dissociation of the C-4–C-5 bond has the lowest rate constant up to very high excitations (>450 kJ mol^{-1}) where the log k_{O-C-2} and log $k_{C-4-C-5}$ curves converge.

Solving the system of differential kinetic equations [55] pertinent to Scheme 4 yielded the molar fractions of **1**, **5**, **7**, and the products, as depicted in Figure 9. The molar fractions are plotted versus internal energy in **1** which was the starting reactant that had x(**1**) = 1 at internal energies below the lowest TS, $E \leq 119$ kJ mol^{-1},

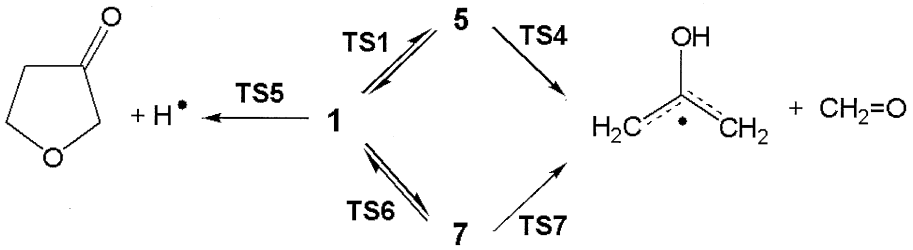

Scheme 4

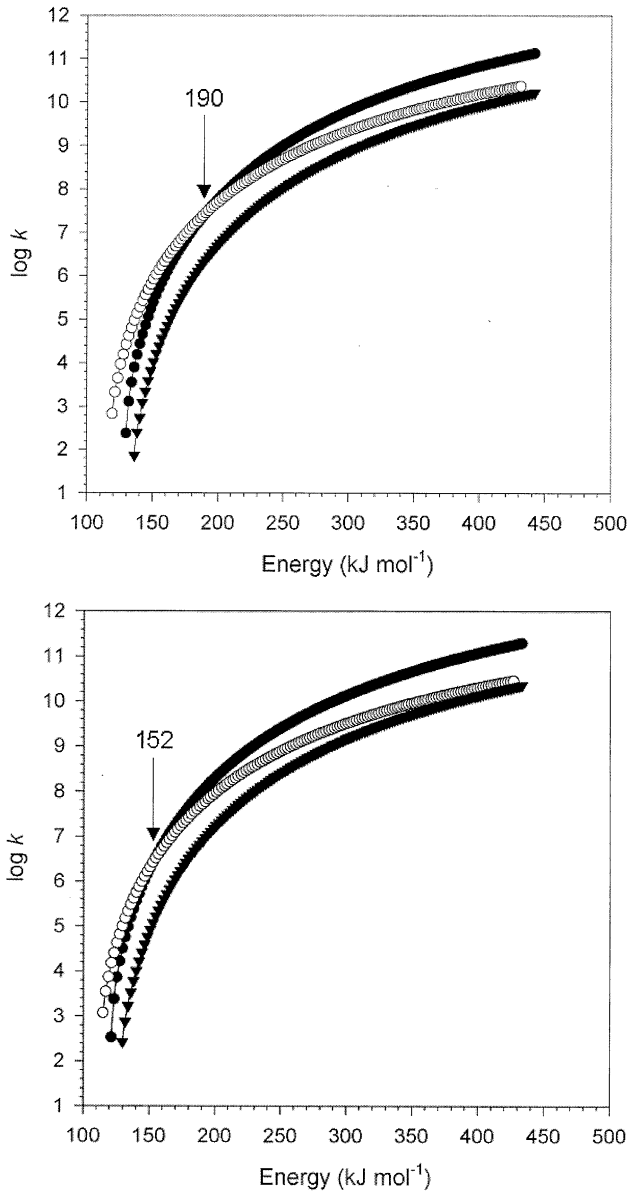

Figure 8. RRKM rate constants (log k, s^{-1}) for dissociations of **1** from (top) G2(MP2) and (bottom) B3-PMP2/6-311 + G(3df,2p) TS energy calculations. Filled circles: O-1–H bond dissociation; open circles: O-1–C-2 bond dissociation; filled triangles: C-4–C-5 bond dissociation.

and at time zero. The dissociation time was set to be equal to the flight time of the neutral intermediates, t = 4.4 μs. The branching ratios show that the reactant **1** rapidly disappears in the energy interval of 130–150 kJ mol^{-1}, while the molar fractions of intermediates **5** and **7** remain very low (<3%) throughout the entire energy range. The molar fractions of the [2-hydroxyallyl radical + CH_2=O] products show a maximum at 155 kJ mol^{-1}, and then decrease at higher energies. The crossing point with the formation of [**2** + H] in Figure 9 coincides with the crossing point of the RRKM rate constants in Figure 8 (190 kJ mol^{-1}).

An estimate of the competitive formations of [**2** + H]

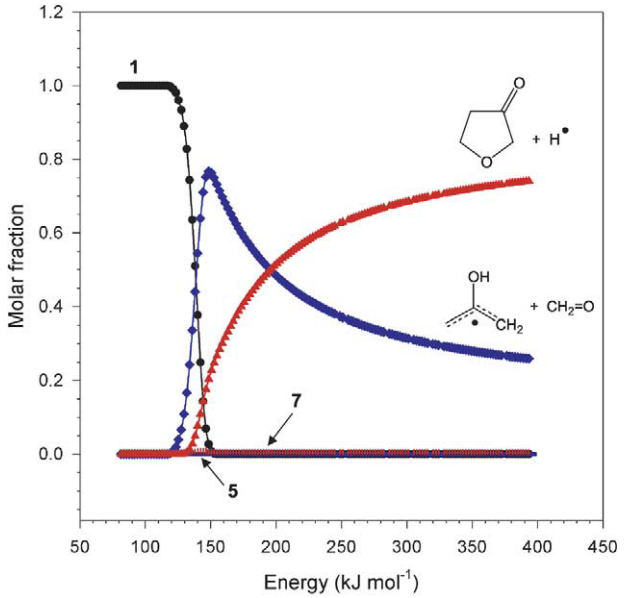

Figure 9. Molar fractions at t = 4.4 μs of **1**, **5**, **7**, [2 + H], and [hydroxyallyl + CH_2=O] calculated according to Scheme 4 using RRKM rate constants that were based on G2(MP2) transition state energies.

and [2-hydroxyallyl + CH_2O] products can be obtained by convoluting the $x(E)$ values with an energy distribution function (eq. 1) [56]. The onset (E_0) and width (W) parameters were chosen as E_0 = 125 and W = 155 kJ mol^{-1}, which give the most probable internal energy in **1** as 203 kJ mol^{-1}, consistent with excitation by vibronic conversion from the first excited state. Although this may appear as an ad hoc assumption, the dissociation kinetics based on these parameters also reproduced the 1.5% fraction of survivor **1** observed experimentally.

$$P(E) = \frac{4(E - E_0)}{W^2} e^{\frac{-2(E-E_0)}{W}} \qquad E \geq E_0 \qquad P(E) = 0$$

$$E \leq E_0 \tag{1}$$

The energy-averaged molar fractions for the products $\langle x \rangle$, calculated by convoluting the $x(E)$ and $P(E)$ functions over the 125–420 kJ mol^{-1} energy interval, allowed us to assess the yields of the most important species at t = 4.4 μs. These were obtained as $\langle x(\mathbf{1}) \rangle$:$\langle x(\mathbf{2}$ + H)$\rangle$:$\langle x$(2-hydroxyallyl + CH_2=O)$\rangle$ = 1.5:56:42 for the rate constants that were based on the G2(MP2) transition state energies. Thus, according to the RRKM analysis, the loss of H from the hydroxyl group is predicted to be the most efficient dissociation of **1** following vertical electron transfer.

Conclusions

The 3-hydroxyoxolan-3-yl radical **1** is a stable species when formed by collisional electron transfer in the gas phase. Vibrationally excited **1** undergoes competitive dis-

sociations by ring-cleavage dissociations forming 2-hydroxyallyl radical and formaldehyde and by loss of the hydroxyl hydrogen atom forming oxolan-3-one. The ring-cleavage dissociations are predicted by ab initio/RRKM calculations to predominate at excitations <190 kJ mol^{-1}. In addition, excited electronic states of **1** undergo ring cleavage dissociations forming C_2H_3O and C_2H_4O neutral species. The isomeric 3-oxo-(*1H*)-oxolanium radical is unstable and undergoes exothermic ring opening that results in elimination of OH radical. Our experimental and computational results show that ring cleavages are the dominant dissociations of 3-hydroxyoxolan-3-yl radical at low vibrational excitations or from excited electronic states. This suggests that similar ring-cleavage dissociations leading to strand breaks can be operative in DNA degradation caused by reactive radicals or UV light.

Acknowledgments

The authors gratefully acknowledge support of this research by the National Science Foundation (grants CHE-0090930 and CHE-0349595 for experiments and CHE-9808181 and CHE-0342956 for computations). The Chemistry Department Computational Facility also received support from the University of Washington. The JEOL HX-110 mass spectrometer was a donation from the former Biomembrane Institute by courtesy of Professor S. Hakomori.

References

1. (a) Duff, R. J.; de Vroom, E.; Geluk, A.; Hecht, S. M.; van der Marel, G. A.; van Boom, J. H. Evidence for C-1′ Hydrogen Abstraction from Modified Oligonucleotides by Iron-Bleomycin. *J. Am. Chem. Soc.* **1993,** *115,* 3350–3351. (b) McGall, G. H.; Rablow, L. E.; Ashley, G. W.; Wu, S. H.; Kozarich, J. W.; Stubbe, J. New Insight into the Mechanism of Base Propenal Formation During Bleomycin-Mediated DNA Degradation. *J. Am. Chem. Soc.* **1992,** *114,* 4958–4967. (c) Hangeland, J. J.; De Voss, J. J.; Heath, J. A.; Townsend, C. A. Specific Abstraction of the 5′S- and 4′-Deoxyribosyl Hydrogen Atoms from DNA by Calicheamicin γ1I. *J. Am. Chem. Soc.* **1992,** *114,* 9200–9202. (d) Zein, N.; Poncin, M.; Nilakantan, R.; Ellestad, G. A. Calicheamicin γ1I and DNA: Molecular Recognition Process Responsible for Site-Specificity. *Science* **1989,** *244,* 697–699. (e) Goldberg, I. H. Mechanism of Neocarzinostatin Action: Role of DNA Microstructure in Determination of Chemistry of Bistranded Oxidative Damage. *Acc. Chem. Res.* **1991,** *24,* 191–198. (f) Myers, A. G.; Cohen, S. B.; Kwon, B. M. DNA Cleavage by Neocarzinostatin Chromophore. Establishing the Intermediacy of Chromophore-Derived Cumulene and Biradical Species and Their Role in Sequence-Specific Cleavage. *J. Am. Chem. Soc.* **1994,** *116,* 1670–1682. (g) Sigman, D. S. Nuclease Activity of 1,10-Phenanthroline-Copper Ion. *Acc. Chem. Res.* **1986,** *19,* 180–186. (h) Cheng, C-C.; Goll, J. G.; Neyhart, G. A.; Welch, T. W.; Singh, P.; Thorp, H. H. Relative Rates and Potentials of Competing Redox Processes during DNA Cleavage: Oxidation Mechanisms and Sequence-Specific Catalysis of the Self-Inactivation of Oxometal Oxidants by DNA. *J. Am. Chem. Soc.* **1995,** *117,* 2970–2980. (i) Neyhart, G. A.; Cheng, C-C.; Thorp, H. H. Kinetics and Mechanism of the Oxidation of Sugars and Nucleotides by Oxoruthenium (IV): Model Studies for Predicting Cleavage Patterns in Polymeric DNA and RNA. *J. Am. Chem. Soc.* **1995,** *117,* 1463–1471. (j) Greenberg, M. M.; Barvian, M. R.; Cook, G. P.; Goodman, B. K.; Matray, T. J.; Tronche, C.; Venkatesan, H. DNA Damage Induced via 5,6-Dihydrothymid-5-yl in Single-Stranded Oligonucleotides. *J. Am. Chem. Soc.* **1997,** *119,* 1828–1839.
2. Burrows, C. J.; Muller, J. G. Oxidative Nucleobase Modifications Leading to Strand Scission. *Chem. Rev.* **1998,** *98,* 1109–1151.
3. von Sonntag, C. *The Chemical Basis of Radiation Damage*; Taylor and Francis: London, 1987.
4. Knapp-Pogozelski, W.; Tullius, T. D. Oxidative Strand Scission of Nucleic Acids: Routes Initiated by Hydrogen Abstraction from the Sugar Moiety. *Chem. Rev.* **1998,** *98,* 1089–1107.
5. Schuchmann, M. N.; von Sonntag, C. Radiation Chemistry of Carbohydrates. Part 14. Hydroxyl Radical Induced Oxidation of D-Glucose in Oxygenated Aqueous Solution. *J. Chem. Soc. Perkin Trans. 2,* **1977,** 1958–1963.
6. Madden, K. P.; Fessenden, R. W. ESR Study of the Attack of Photolytically Produced Hydroxyl Radicals on α-Methyl-D-Glucopyranoside in Aqueous Solution. *J. Am. Chem. Soc.* **1982,** *104,* 2578–2581.
7. Kochetkov, N. K.; Kudrjashov, L. I.; Chlenov, M. A. *Radiation Chemistry of Carbohydrates*; Pergamon Press: Oxford, 1979.
8. Meschwitz, S. M.; Schultz, R. G.; Ashley, G. W. Goldberg, I. H. Selective Abstraction of Deuterium from C-1′ of the C Residue in AGC.ICT by the Radical Center at C-2 of Activated Neocarzinostatin Chromophore: Structure of the Drug/DNA Complex Responsible for Bistranded Lesion Formation. *Biochemistry* **1992,** *31,* 9117–9121.
9. Pitie, M.; Bernadou, J.; Meunier, B. Oxidation at Carbon-1′ of DNA Deoxyriboses by the Mn-TMPyP/KHSO5 System Results from a Cytochrome *P*-450-type Hydroxylation Reaction. *J. Am. Chem. Soc.* **1995,** *117,* 2935–2936.
10. Kappen, L. S.; Goldberg, I. H. Identification of 2-Deoxyribonolactone at the Site of Neocarzinostatin-Induced Cytosine Release in the Sequence d(AGC). *Biochemistry* **1989,** *28,* 1027–1032.
11. Goyne, T. E.; Sigman, D. S. Nuclease activity of 1,10-Phenanthroline-Copper Ion. Chemistry of Deoxyribose Oxidation. *J. Am. Chem. Soc.* **1987,** *109,* 2846–2848.
12. Goodman, B. K.; Greenberg, M. M. Independent Generation and Reactivity of 2′-Deoxyurid-1′-yl. *J. Org. Chem.* **1996,** *61,* 2–3.
13. Deycard, S.; Lusztyk, J.; Ingold, K. U.; Zerbetto, F.; Zgierski, M. Z.; Siebrand, W. Inversion of the Dioxolanyl Radical: An Experimental and Theoretical Study. *J. Am. Chem. Soc.* **1990,** *112,* 4284–4290.
14. Malatesta, V.; Ingold, K. U. Kinetic Applications of Electron Paramagnetic Resonance Spectroscopy. 36. Stereoelectronic Effects in Hydrogen Atom Abstraction from Ethers. *J. Am. Chem. Soc.* **1981,** *103,* 609–614.
15. Beckwith, A. L. J.; Easton, C. J. Stereoelectronic Effects in Hydrogen Atom Abstraction from Substituted 1,3-Dioxanes. *J. Am . Chem. Soc.* **1981,** *103,* 615–619.
16. For the most recent reviews of the technique see: (a) Turecek, F. Transient Intermediates of Chemical Reactions by Neutralization-Reionization Mass Spectrometry. *Top. Curr. Chem.* **2003,** *225,* 77–129. (b) Zagorevskii, D. V.; Holmes, J. L. Neutralization-Reionization Mass Spectrometry Applied to Organometallic and Coordination Chemistry (Update: 1914–1998). *Mass Spectrom. Rev.* **1999,** *18,* 87–118. (c) Schalley, C. A.; Hornung, G.; Schroder, D.; Schwarz, H. Mass Spectrometric Approaches to the Reactivity of Transient Neutrals. *Chem. Soc. Rev.* **1998,** *27,* 91–104.
17. Nguyen, V. Q.; Tureček, F. Protonation Sites in Gaseous Pyrrole and Imidazole and the Stabilities of Their Radicals. *J. Mass Spectrom.* **1996,** *31,* 1173–1184.
18. Nguyen, V. Q.; Tureček, F. Gas-Phase Protonation of Pyridine. A Variable-Time Neutralization-Reionization and Ab Initio Study of Pyridinium Radicals. *J. Mass Spectrom.* **1997,** *32,* 55–63.
19. Nguyen, V. Q.; Tureček, F. Protonation Sites in Pyrimidine and Pyrimidinamines in the Gas Phase. *J. Am. Chem. Soc.* **1997,** *119,* 2280–2290.

20. Wolken, J. K.; Syrstad, E. A.; Vivekananda, S.; Tureček, F. Uracil Radicals in the Gas Phase. Specific Generation and Energetics. *J. Am. Chem. Soc.* **2001,** *123,* 5804–5805.
21. Syrstad, E. A. ; Vivekananda, S.; Tureček, F. Direct Observation of a Hydrogen Atom Adduct to C-5 in Uracil. A Neutralization-Reionization Mass Spectrometric and ab Initio Study. *J. Phys. Chem. A* **2001,** *105,* 8339–8351.
22. Wolken, J. K.; Tureček, F. Direct Observation of a Hydrogen Atom Adduct to O-4 in Uracil. A Neutralization-Reionization Mass Spectrometric and ab Initio Study. *J. Phys. Chem. A* **2001,** *105,* 8352–8360.
23. Tureček, F.; Gu, M.; Hop, C. E. C. A. Franck-Condon Dominated Chemistry. Formation and Dissociations of Tetrahydroxyphosphoranyl Radicals Following Femtosecond Reduction of Their Cations in the Gas Phase. *J. Phys. Chem.* **1995,** *99,* 2278–2291.
24. Tureček, F. Modeling Nucleobase Radicals in the Mass Spectrometer. *J. Mass Spectrom.* **1998,** *33,* 779–795.
25. Vivekananda, S.; Sadilek, M.; Chen, X.; Tureček, F. Modeling Deoxyribose Radicals by Neutralization-Reionization Mass Spectrometry. Part 1. Preparation, Dissociations, and Energetics of 2-Hydroxyoxolan-2-yl Radical, Neutral Isomers, and Cations. *J. Am. Soc. Mass Spectrom.* **2004,** *15,* preceding paper in this issue.
26. Holmes, J. L. The Neutralization of Organic Cations. *Mass Spectrom. Rev.* **1989,** *8,* 513–539.
27. Taylor, E. C.; Macor, J. E. Synthesis of Pyridines by Diels-Alder Reactions of Hetero-Substituted 1,2,4-Triazines with Enamines and an Enaminone. *J. Org. Chem.* **1989,** *54,* 1249–1256.
28. Tureček, F.; Gu, M.; Shaffer, S. A. A Novel Tandem Quadrupole Acceleration-Deceleration Mass Spectrometer for Neutralization-Reionization Studies. *J. Am. Soc. Mass Spectrom.* **1992,** *3,* 493–501.
29. Kuhns, D. W.; Shaffer, S. A.; Tran, T. B.; Tureček, F. The Methylthiomethyl Radical. A Variable-Time Neutralization-Reionization and ab Initio Study. *J. Phys. Chem.* **1994,** *98,* 4845–4853.
30. Kuhns, D. W.; Tureček, F. Unimolecular Neutral and Ion Kinetics by Variable-Time Neutralization-Reionization Mass Spectrometry. *Org. Mass Spectrom.* **1994,** *29,* 463–469.
31. Frisch, M. J.; Trucks, G. W.; Schlegel, H. B.; Scuseria, G. E.; Robb, M. A.; Cheeseman, J. R.; Zakrzewski, V. G.; Montgomery, J. A.; Stratmann, R. E.; Burant, J. C.; Dapprich, S.; Millam, J. M.; Daniels, A. D.; Kudin, K. N.; Strain, M. C.; Farkas, O.; Tomasi, J.; Barone, V.; Cossi, M.; Cammi, R.; Mennucci, B.; Pomelli, C.; Adamo, C.; Clifford, S.; Ochterski, J.; Petersson, G. A.; Ayala, P. Y.; Cui, Q.; Morokuma, K.; Malick, D. K.; Rabuck, A. D.; Raghavachari, K.; Foresman, J. B.; Cioslowski, J.; Ortiz, J. V.; Stefanov, B. B.; Liu, G.; Liashenko, A.; Piskorz, P.; Komaromi, I.; Gomperts, R.; Martin, R. L.; Fox, D. J.; Keith, T.; Al-Laham, M. A.; Peng, C. Y.; Nanayakkara, A.; Gonzalez, C.; Challacombe, M.; Gill, P. M. W.; Johnson, B. G.; Chen, W.; Wong, M. W.; Andres, J. L.; Head-Gordon, M.; Replogle, E. S.; Pople, J. A. Gaussian 98, Revision A.6; Gaussian, Inc.: Pittsburgh PA, 1998.
32. (a) Becke, A. D. A New Mixing of Hartree-Fock and Local-Density-Functional Theories. *J. Chem. Phys.* **1993,** *98,* 1372–1377. (b) Becke, A. D. Density-Functional Thermochemistry. III. The Role of Exact Exchange. *J. Chem. Phys.* **1993,** *98,* 5648–5652.
33. Stephens, P. J.; Devlin, F. J.; Chabalowski, C. F.; Frisch, M. J. Ab Initio Calculation of Vibrational Absorption and Circular Dichroism Spectra Using Density Functional Force Fields. *J. Phys. Chem.* **1994,** *98,* 11623–11627.
34. Mayer, I. Spin-projected EHF method. IV. Comparison of Potential Curves Given by Different One-Electron Methods. *Adv. Quantum Chem.* **1980,** *12,* 189–262.
35. Schlegel, H. B. Potential Energy Curves Using Unrestricted Moeller-Plesset Perturbation Theory with Spin Annihilation. *J. Chem. Phys.* **1986,** *84,* 4530–4534.
36. Rauhut, G.; Pulay, P. Transferable Scaling Factors for Density Functional Derived Vibrational Force Fields. *J. Phys. Chem.* **1995,** *99,* 3093–3100.
37. Curtiss, L. A.; Raghavachari, K.; Pople, J. A. Gaussian-2 Theory Using Reduced Moeller-Plesset Orders. *J. Chem. Phys.* **1993,** *98,* 1293–1298.
38. Pople, J. A.; Head-Gordon, M.; Raghavachari, K. Quadratic Configuration Interaction. A General Technique for Determining Electron Correlation Energies. *J. Chem. Phys.* **1987,** *87,* 5968–5975.
39. Møller, C.; Plesset, M. S. Note on an Approximation Treatment for Many-Electron Systems. *Phys. Rev.* **1934,** *46,* 618–622.
40. Tureček, F.; Yao, C. Hydrogen Atom Addition to Cytosine, 1-Methylcytosine, and Cytosine-Water Complexes. A Computational Study of a Mechanistic Dichotomy. *J. Phys. Chem A* **2003,** *107,* 9221–9231.
41. Tureček, F.; Syrstad, E. A. Mechanism and Energetics of Intramolecular Hydrogen Transfer Atom Transfer in Amide and Peptide Radicals and Cation-Radicals. *J. Am. Chem. Soc.* **2003,** *125,* 3353–3369.
42. Tureček, F.; Vivekananda, S.; Sadílek, M.; Polášek, M. Lactone Enol Cation-Radicals: Gas-Phase Generation, Structure, Energetics, and Reactivity of the Ionized Enol of Butane-4-lactone. *J. Mass Spectrom.* **2002,** *37,* 829–839.
43. Tureček, F. Proton Affinity of Dimethyl Sulfoxide and Relative Stabilities of C_2H_6OS Molecules and $C_2H_7OS^+$ Ions. *J. Phys. Chem. A* **1998,** *102,* 4703–4713.
44. Stratmann, R. E.; Scuseria, G. E.; Frisch, M. J. An Efficient Implementation of Time-Dependent Density-Functional Theory for the Calculation of Excitation Energies of Large Molecules. *J. Chem. Phys.* **1998,** *109,* 8218–8224.
45. Zhu, L., Hase, W. L. *Quantum Chemistry Program Exchange*; Indiana University: Bloomington, IN, 1994; Program No. QCPE 644.
46. Frank, A. J.; Sadílek, M.; Ferrier, J. G.; Tureček, F. Sulfur Oxyacids and Radicals in the Gas Phase. A Variable-Time Neutralization-Photoexcitation-Reionization Mass Spectrometric and ab Initio/RRKM Study. *J. Am. Chem. Soc.* **1997,** *119,* 12343–12353.
47. *NIST Standard Reference Database* No. 69; February 2000 Release; http//:webbook.nist.gov.
48. Raksit, A. B.; Porter, R. F. Direct Experimental Observations of Metastability in the (Dideuterio)Methyloxonium Radical. *J. Chem. Soc. Chem. Commun.* **1987,** 500–501.
49. Wesdemiotis, C.; Fura, A.; McLafferty, F. W. Protonated Ethanol and Its Neutral Counterparts. *J. Am. Soc. Mass Spectrom.* **1991,** *2,* 459–463.
50. Holmes, J. L.; Sirois, M. Hypervalent Radicals; the Generation of $CH_3O(H)CH_3$, $CH_3O(H)C_2H_5$ and their O-(D) Analogs by Neutralization of the Corresponding Cations. *Org. Mass Spectrom.* **1990,** *25,* 481–482.
51. Sadílek, M.; Tureček, F. Probing Hypervalent Radicals by Neutralization-Laser Photoionization Mass Spectrometry. *J. Phys. Chem.* **1996,** *100,* 9610–9614.
52. Tureček, F.; Reid, P. J. Metastable States of Dimethyloxonium, $(CH_3)_2OH^{\cdot}$. *Int. J. Mass Spectrom.* **2003,** *222,* 49–61.
53. Dua, S.; McAnoy, A. M.; Blumenthal, T.; Bowie, J. H. Does the Radical $Me_3O^{\cdot}$ Exist in the Gas Phase? A Joint Experimental and Theoretical Study. *Int. J. Mass Spectrom.* **2003,** *230,* 77–84.
54. Tureček, F. The Modern Mass Spectrometer. A Laboratory for Unstable Neutral Species. *Org. Mass Spectrom.* **1992,** *27,* 1087–1097.
55. *Mathematica, Version 5.0*; Wolfram Research, Inc.: Champaign, IL, 2003.
56. Tureček, F. The Use of Kinetic Isotope Effects for the Determination of Internal Energy Distributions of Isolated Transient Species in the Gas Phase. *Int. J. Mass Spectrom.* **2003,** *227,* 327–338.